

Monte-Carlo Science

Javier Jiménez*

School of Aeronautics, Universidad Politécnica Madrid, 28040 Madrid, Spain

March 8, 2020

Abstract

This paper explores how far the scientific discovery process can be automated. Using the identification of causally significant flow structures in two-dimensional turbulence as an example, it probes how far the usual procedure of planning experiments to test hypotheses can be substituted by ‘blind’ randomised experiments, and notes that the increased efficiency of computers is beginning to make such a ‘Monte-Carlo’ approach practical in fluid mechanics. The process of data generation, classification and model creation is described in some detail, stressing the importance of validation and verification. Although the purpose of the paper is to explore the procedure, rather than to model two-dimensional turbulence, it is encouraging that the Monte Carlo process naturally leads to the consideration of vortex dipoles as building blocks of the flow, on a par with the more conventional individual vortex cores. Although not completely novel, this ‘spontaneous’ discovery supports the claim that an important advantage of randomised experiments is to bypass researcher prejudice and alleviate paradigm lock. It is finally noted that the method can be extended to three-dimensional flows in practical times.

1 Introduction

The business of science is to search for laws that can be used to make predictions. As such, the classical point of view is that a prerequisite for science is the determination of causal relations (*Does A cause B?*), preferably complemented by mechanisms (*How A causes B?*). Both are important. Causality without mechanisms is unlikely to lead to quantitative predictions, and mechanisms without causality have a high probability of being wrong. Both have to be testable, preferably using different data from their training sets. For example, the ancient Greeks invented causes and mechanisms involving gods and chariots for the alternation of night and day. They fitted the known facts well, but we know today that they are hard to generalise.

There are two meanings of the word ‘science’. The first one is a systematic method for discovering how things work [1], and the second is the resulting body of knowledge about how they work [2]. Depending of who you ask, one aspect is considered more important than the other but, without taking sides in this dichotomy, this paper deals mostly with methodological

*CONTACT Javier Jiménez. Email: javier.jimenezs@upm.es

aspects. Its contribution to the body of knowledge of fluid mechanics is not intended to be major.

In particular, we explore how to determine causality in physical systems, and whether recent developments provide new ways of doing so. To fix ideas, we illustrate our argument with the study of a particularly flow – two-dimensional decaying homogeneous turbulence – about which the general feeling is that most things are understood. As such, we will be able to test our conclusions against accepted wisdom, although this may lead some readers to think that the discussion is uninteresting, because nothing new is likely to be discovered. We will see that this is not quite true. Some new aspects can still be unearthed, or at least rediscovered, and the method for doing so is interesting because it would not have been practical a decade ago.

Similarly, other readers could be excused for wondering why a paper dealing with apparently philosophical questions about causality, and centred on an unfashionable flow, should be included in a special issue on the use of artificial intelligence (AI) in fluid mechanics. In a sense, they would be right. Artificial intelligence, as the term is mostly used at the moment, is a collection of techniques for the exploitation of large quantities of data. In terms of the scientific method, this corresponds to the generation of empirical knowledge, which is only one of several steps in scientific exploration. What interests us here is the full process of data exploitation, from their generation to their final incorporation into hypotheses. It will become clear that AI is only occasionally useful in the process, mainly as a tool, but that computers are indispensable at most stages of it.

There are several distinctions to be made before we begin our argument. The first one has to do with how AI is supposed to work [3], which is traditionally divided into *symbolic* [4] and *sub-symbolic* [5]. Symbolic AI is the classical kind, which manipulates symbols representing real-world variables according to rules set by the programmer, typically embodied into an ‘expert system’. For example, assuming some personal definition of vortices, AI can be used to encapsulate this knowledge into rules to identify and isolate them. On the contrary, sub-symbolic AI is not interested in rules, but in algorithms to do things. For example, given enough snapshots of a flow in which vortices have been identified (maybe by a pre-existing expert system) we can train a neural network to distinguish them from vorticity sheets. The result of sub-symbolic AI is not the rule, but the algorithm, and it does not imply that a rule exists. After training our system, we may not know (or care) what a vortex is, or what distinguishes it from a sheet, but we may have a faster way of distinguishing one from the other than what would have been possible using only pre-ordained physics-based rules. Copernicus and the Greeks had symbolic representations of the day-night cycle, although with very different ideas of the rules involved. Most other living beings, which can distinguish night from day and usually predict quite accurately dawn and dusk, are (probably) sub-symbolic. The classical scientific method, including causality, is firmly on the symbolic side of the divide: we are not only interested in the result, but also in the rule. But there is a small but growing body of scientists and engineers, who feel that data and a properly trained algorithm are all the information required about Nature, and that no further rule is necessary, as for example discussed in [6,7].

Engineering and medicine have always been at least partly empirical and data-driven, but biochemistry was probably the first subject to reach the sub-symbolic level in modern times, after fast methods of DNA synthesis became available in the 1980s. Much of the modern discussion on raw empiricism relates to it [8], and so did the first article claiming to describe a ‘robot scientist’ [9]. The availability of enough data to even consider sub-symbolic fluid mechanics was only recently made possible by the numerical simulations of the 1990’s, which gave us for the first time the feeling that ‘we knew everything’, and that any question that

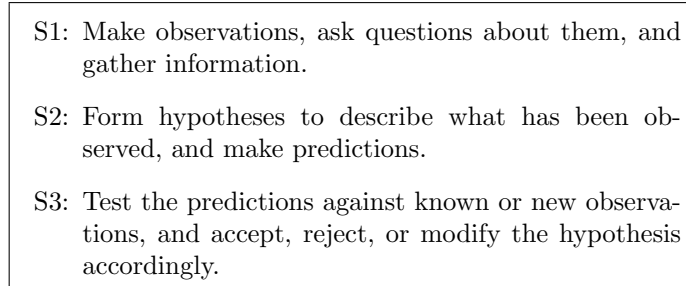


Figure 1: The scientific method

could be posed to a computer would eventually be answered [10,11]. Of course, even without practical considerations of cost, this did not mean that all questions were answered, because they first had to be put to the computer by a researcher.

In this paper we discuss to what extent this last roadblock can be removed. The new enabling technology is the increased speed and memory capacity of computers, which can do in minutes what used to take days a decade ago. We will argue that this enables a new way of asking questions, not based on plausible hypothesis, but randomly, in the hope that some of them might turn out to be interesting. This ‘Monte Carlo’ procedure does not avoid the necessity of answering the questions, which can presumably also be done by the computer, nor of evaluating how ‘interesting’ are the answers, which most probably computers cannot yet do. It neither points towards a future of ‘human-less’ research, but to a new level of partnership between humans and computers. Similar steps have been taken before: we no longer dig canals or throw spears by hand, except as a sport, nor do we do arithmetic with pencil and paper, or integrate differential equations using special functions. Most of these human-machine symbioses are usually considered beneficial, although many created their own disruptions when they were introduced. There is no reason to believe that this time will be different, but it is fair to question which the new advantages and difficulties will be.

Relinquishing control of the questions to be asked is not an altogether new experience to anybody who has trained graduate students, mentored postdocs, or managed an industrial or academic research group. Any such person knows the feeling that, at some point, the research is no longer yours, although most of us console ourselves by arguing that we are training our peers and that, in the end, the overall direction is set by us. Monte Carlo science lacks both of these (probably spurious) consolations. This may be its main advantage. It is inevitable that our students or subordinates share some of our ideas and, most probably, some of our prejudices. It is often argued that researcher prejudice is the main roadblock to qualitative scientific advances, and that ‘paradigm shifts’, always hard to come by, are delayed by it [2]. The main advantage to be gained from a Monte-Carlo questioning algorithm is probably its lack of prejudice. If we can avoid transferring our biases to it, such an algorithm would act as an efficient, *unprejudiced*, although probably not yet very smart, scientific assistant.

There is a second distinction that, although related to the previous one, is independent from it. We have mentioned the importance of causes, but research is not always geared towards them. The classical description of the scientific method is summarised in figure 1, which emphasised its iterative character. The causal relations mentioned above are encapsulated in the modelling and testing steps, S2 and S3, and emphasis is often put on them rather than on the data-gathering step S1. In fact, the research loop is often started in S2, and only later are hypotheses

tested against observations, as in S2–S1–S3. The implied relation is not always causal. Even in data-driven research, where observations precede hypotheses, the argument is often that “if A precedes B”, A is likely to be the cause of B, although it is generally understood that correlation and causation are not equivalent. A classical example is the observation of night and day mentioned above. The correlation between earlier days and later nights is perfect, but it does not imply causation [12].

On the other hand, the concept of causality is not without problems, and it has been argued that it is indistinguishable from initial conditions in systems described by differential equations, such as fluid mechanics [13]. While this is true, and we could frame our goal as a quest to classify initial conditions in terms of their outcome, the result may not be very informative. We will restrict ourselves here to a shorter-term definition of the type of: “The falling tree causes the crashing noise”, even if we know that the fall of the tree has its own reasons for happening, and that such intermediate causes depend on the time horizon that we impose on them. Such conclusions require something beyond correlations, and imply an active intervention of the observer in the generation of data to interrupt the flow of causality from the notional ‘original’ cause into something more immediate. This is particularly important in turbulence and other chaotic systems, especially if we want to retain some control authority in spite of the loss of system memory.

Simplifying a lot, the difference between the two points of view, which mostly affects how and when step S1 is undertaken in figure 1, can be summarised as that *observational* science searches for correlations between observations, and generalises them into models. It is the science of prediction, and is sub-symbolic at heart.

On the contrary, *interventional* science relies on the results of experiments in which some condition is changed by the observer, generally in the hope of uncovering ‘causal’ (i.e., if this, then that), or ‘counterfactual’ relations (if not this, then not that) [14]. It is the science of control, and usually at least aims for symbolic intelligence.

The present paper is oriented towards control. In the example above, we care about the falling tree because we might want to prevent it from making noise. A prediction paper would worry more about establishing correlations between tree health and noise levels, without being especially interested in causality, and would be very different from the present one.

The rest of the paper is structured as follows. Section §2 describes how the Monte Carlo ideas in this introduction can be applied to the particular problem of two-dimensional turbulence, and §3 briefly discusses the physics that can be learned from them. The paper closes in §4 with a discussion of the connections that can be established between the scientific method and modern data analysis, in the light of the experience of the previous two sections. Two appendices collect implementation details required by those interested in reproducing the experiments in §2. Appendix A describes how the temporal horizon of our causal perturbations is chosen, and appendix B explains how to impose perturbations on vector properties, such as the velocity.

2 Causality in two-dimensional turbulence: a case study

Two-dimensional turbulence is an old problem in fluid mechanics, often discussed in relation with geophysical flows [15]. It also appears naturally in highly stratified situations, which tend to collapse eddies into almost two-dimensional pancakes [16], and has more recently been

Case	Perturbation to cell	Symbol
0	$\omega \Rightarrow 0$	$-\circ$
1	$\omega \Rightarrow -\text{r.m.s.}_c(\omega)$	$-\triangle$
2	$\omega \Rightarrow -\omega$	$-\nabla$
3	$\omega \Rightarrow \omega - \langle \omega \rangle_c$, rescaled to keep $\text{r.m.s.}_c(\omega)$ constant.	$-\triangleright$
4	$\omega \Rightarrow -\omega + \langle \omega \rangle_c$, rescaled to keep $\text{r.m.s.}_c(\omega)$ constant.	$-\triangleleft$
10	$\mathbf{u} \Rightarrow 0$	$--\circ$
11	$\mathbf{u} \Rightarrow -\text{r.m.s.}_c(\mathbf{u})$	$--\triangle$
12	$\mathbf{u} \Rightarrow -\mathbf{u}$	$--\nabla$
13	$\mathbf{u} \Rightarrow \mathbf{u} - \langle \mathbf{u} \rangle_c$, rescaled to keep $\text{r.m.s.}_c(\mathbf{u})$ constant.	$--\triangleright$
14	$\mathbf{u} \Rightarrow -\mathbf{u} + \langle \mathbf{u} \rangle_c$, rescaled to keep $\text{r.m.s.}_c(\mathbf{u})$ constant.	$--\triangleleft$
15	$\mathbf{u} \Rightarrow +\text{r.m.s.}_c(\mathbf{u})$.	$--\square$

Table 1: Case identification for initial perturbations. In all cases, the mean velocity and vorticity over the full computational box are zeroed after the perturbation is applied. The signs in the substitutions are with respect to the original cell vorticity or velocity. Which velocity component is modified is optimised as in appendix B. When modifying \mathbf{u} , an extra continuity ‘pressure’ step is applied, which may substantially modify the perturbation. The ‘c’ subindex labels statistics over a single cell.

studied in Bose–Einstein condensates [17]. It fundamentally differs from three-dimensional turbulence in that the absence of vortex stretching inhibits the generation of velocity gradients, and therefore the usual energy cascade [18]. In the inviscid limit, both energy and enstrophy are conserved. Early papers centred on the statistical consequences of these conservation laws, and made predictions that were approximately satisfied [19–21], but it was soon realised that another consequence of the additional conservation law is the formation of coherent vortex cores [22–24], whose presence interferes with the regular statistical cascade [25]. Since that realisation, the temporal evolution of two-dimensional turbulence has mostly been described in terms of the behaviour of these vortices [26–28]. General reviews can be found in [29,30]

We discuss in this section how Monte-Carlo experimentation can be applied to test whether this vortex model is the only possible one for causality in two-dimensional decaying turbulence. The problem and the general procedure are described in [11,31], and there are few differences between the experiments here and in these references. The new material mostly refers to postprocessing the resulting data, and to how conclusions can be drawn from them.

The method can be summarised as follows. A number (N_{exp}) of experimental flow fields (‘flows’ from now on) are prepared, and each of them is perturbed in various ways (‘experiments’ from now on) to create initial conditions. Each experiment is run for a prescribed time that varies between $\omega'_0 T = 10$ and 30 turnovers, where $\omega'_0 = \langle \omega^2 \rangle^{1/2}$ is the root-mean-square (r.m.s.) vorticity of the initial unperturbed flow, and the time-dependent average $\langle \cdot \rangle$ is taken over the full computational box. As the evolution of the perturbed flow diverges from that of the unperturbed initial condition, their difference is stored at several test times. The magnitude of the evolving perturbation is defined as the norm, $\epsilon(t)$, of the difference between the perturbed and unperturbed flow fields, evaluated over the entire computational box, and the experiments for which this magnitude is largest are defined as most ‘significant’. Four norms are used for this paper: $\| \cdot \|_2$ (quadratic) and $\| \cdot \|_\infty$ (maximum point-wise magnitude), each of them applied to the (scalar) vorticity or to the (vector) velocity. For each case and test time, the n_{keep} perturbations with the largest and smallest deviations are classified as most or least significant, respectively, because, in common with many complex systems, it is empirically found

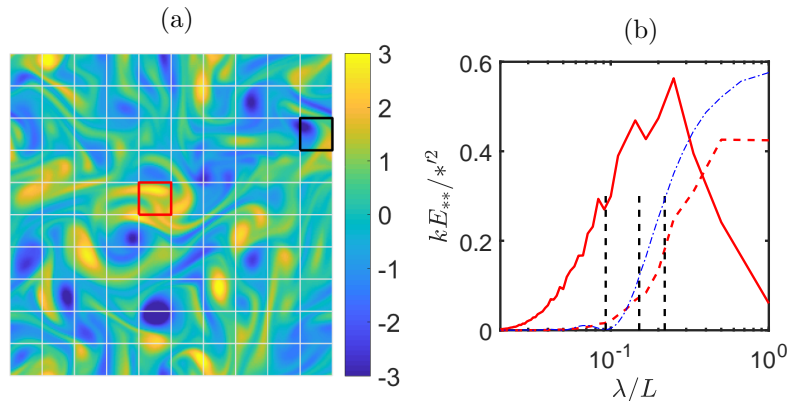


Figure 2: (a) Initial vorticity field used for the evolutions in figure 3. Case 0 in table 1, and $\|u\|_2$ norm used for classification. The cells outlined in black (less significant) and red (more significant) have relatively similar initial perturbation intensities, but very different later evolutions. (b) Premultiplied spectra of the initial flow fields used for the experiments. The dashed vertical lines are the first minimum of the transfer function of a box convolution window corresponding to the cell size of experiments with $N_c = 10, 6$ and 4 , from left to right. —, Enstrophy spectrum; ---, energy; - - - -, transfer function for $N_c = 10$, scaled to fit the plot.

that the first few most- and least-significant experiments result in fairly similar perturbation intensities [32]. Because significance is defined as the effect on the flow at some future time, the most significant experiments are also defined as being most ‘causally important’ for the flow evolution. In our study, the initial perturbation is applied by dividing each flow into a regular grid of $N_c \times N_c$ square cells, each of which is in turn modified in a number of different ways listed in table 1. In most cases, the results are averaged over $N_{exp} = 768$ flows, on a grid with $N_c = 10$ and $n_{keep} = 5$.

Simulations are performed in a doubly periodic square box of side $L = 2\pi$, using a standard spectral Fourier code dealiased by the 2/3 rule. Time advance is third-order Runge-Kutta. The flow is defined by its velocity field $\mathbf{u} = (u, v)$ as a function of the spatial coordinates $\mathbf{x} = (x, y)$, and time. The scalar vorticity is $\omega = \partial_x v - \partial_y u$, and the rate-of-strain tensor is $s_{ij} = (\partial_i u_j + \partial_j u_i)/2$, where the subindices of the partial derivatives range over (x, y) , and those of the velocity components over (u, v) . The rate-of-strain magnitude is defined as $S^2 = 2s_{ij}s_{ij}$, where repeated indices imply summation. Time and velocity are respectively scaled with ω'_0 , and with $q'_0 = (u'^2 + v'^2)^{1/2}$, both measured at the unperturbed initial time, $t = 0$. Unless otherwise specified, all the cases discussed here have Fourier resolution 256^2 , with $Re = q'_0 L / \nu = 2500$, where ν is the kinematic viscosity. Further details can be found in [31].

Figure 2 is a typical initial vorticity field, with the 10×10 grid overlaid. The cell outlined in red is one of the most significant ones, and the one outlined in black is one of the less significant. Both are modified as in case 0 in table 1 (i.e., zeroing the vorticity in the cell), and classified using the $\|u\|_2$ norm. These two cells have been chosen so that they have similar initial perturbation intensities but fairly different intensities at the classification time, $\omega'_0 T_{ref} = 4.5$. The evolution in physical space of their perturbations is shown in figure 3. It is clear that the difference in their temporal evolution is real, and not a global artefact (e.g., such as a different decay rate of the turbulence intensities in the two flows). The significant perturbation rearranges the flow in its vicinity, and its effect eventually spreads to the full field, while the less significant one stays localised and decays.

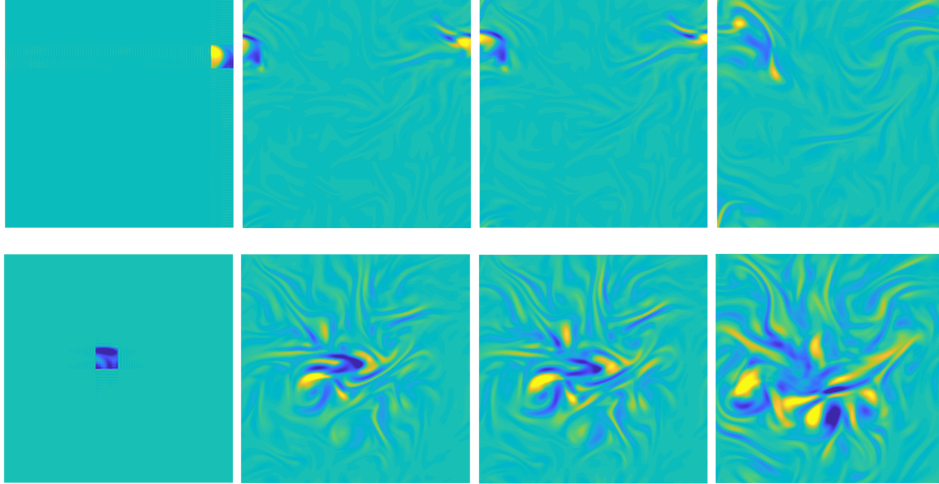


Figure 3: Evolution of the perturbation vorticity for the two cells marked in figure 2. The top row is the less significant cell, marked in black in figure 2. The bottom row is the more significant cell, marked in red. From left to right: $\omega'_0 t = 0, 1.3, 2.6, 4.5$.

The spreading rate of the different perturbations is quantified in figure 4, which measures the geometrical size of the perturbation field as the ratio between their integral quadratic and point-wise norms, normalised in the figure by the size of the cells, L_c . Although the velocity and vorticity norms give slightly different quantitative results, both agree that perturbations start with sizes of the order of the cell size, and spread in times of the order of 5 – 10 turnovers, and that significant perturbations spread faster than non-significant ones. Recalling that $10L_c$ is the size of the computational box, it is clear that individual perturbations have lost most of their individuality over times, $\omega'_0 t \approx 30$, of the order of the longest experiments in the figure.

The purpose of our subsequent analysis is to determine which properties of the unperturbed initial cells best correlate with the magnitude of the effect of modifying them. Several factors are important, such as the modification method (table 1), the norm used to measure the perturbation intensity, and the time T_{ref} at which the classification is done. The following analysis mostly uses the kinetic-energy norm $\|\mathbf{u}\|_2$ as a measure of intensity, and a reference time $\omega'_0 T_{ref} = 4.5$ for the classification, but similar experiments were repeated using $\|\mathbf{u}\|_\infty$, $\|\omega\|_2$ and $\|\omega\|_\infty$, with little difference in the results. The choice of T_{ref} is discussed in appendix A, and its effect on the results, in §2.2 and in figure 8. The properties of each cell used as diagnostic variables are the average cell enstrophy, $\omega_c^2 = \langle \omega^2 \rangle_c$, defined by averaging over individual cells, the averaged kinetic energy, $q_c^2 = \langle u^2 + v^2 \rangle_c$, and the average magnitude of the rate-of-strain tensor, $S_c^2 = \langle S^2 \rangle_c$. The classification scheme in references [11,31] diagnosed significance using an optimal threshold computed for each of these variables in isolation. Each cell was classified as significant or not according to the flow behaviour at T_{ref} , and the resulting labelled set was used to train the threshold in such a way that the number of misclassified events was minimised. In the present case we use a multivariable version of the same idea (support-vector machines [SVM, 33] implemented by the `fitcsvm` Matlab routine), which determines a separating hyperplane instead of a scalar threshold (see figure 5).

The efficiency of the classifier, defined as the fraction of correctly classified events, is collected in the tables in figure 6 for various experimental perturbations and combinations of diagnostic

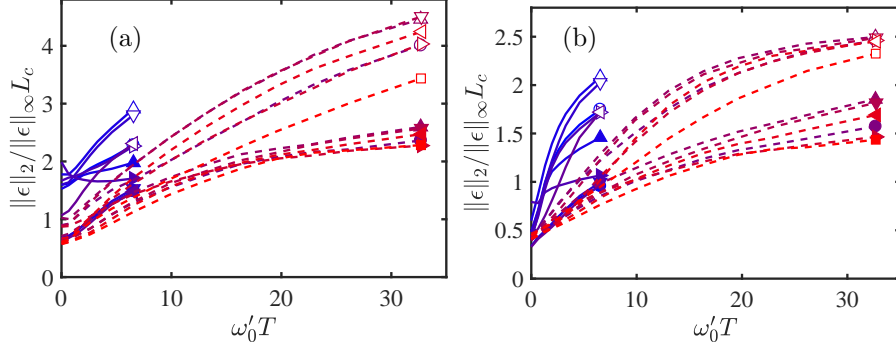


Figure 4: Geometric size of the perturbation as a function of time. Symbols as in table 1, but open symbols are for significant perturbations, and closed ones are for non-significant ones. (a) Compiled using $\|\mathbf{u}\|$. (b) $\|\omega\|$. Note that the definition of significance in this figure is applied independently each test time, so that significant cells are not necessarily the same ones along each line (but see figure 8 below). Lines as in table 1.

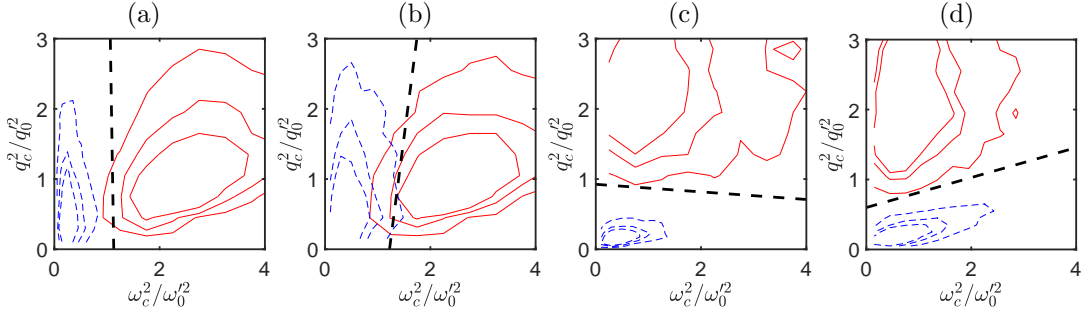


Figure 5: Optimum classification lines for different initial perturbations, in terms of the kinetic energy and of the enstrophy. (a) Case 0. (b) Case 3. (c) Case 10. (d) Case 13. In all cases, 768 flows. Classification norm, $\|\mathbf{u}\|_2$. $N_c = 10$, $n_{keep} = 5$. The contour lines contain 50%, 70% and 90% of the joint probability density functions (p.d.f.) of the diagnostic variables for: —, most significant cases; ---, least significant cases.

variables. It is clear that some linear combination of enstrophy and kinetic energy is always able to separate the data almost perfectly, but that S_c rarely helps. The best combination of vorticity and velocity used by the classifier depends on the initial perturbation method, as shown by the four cases in figure 5. In general, the enstrophy is the best diagnostic variable for perturbations that manipulate the vorticity (case 0 in figure 5.a and case 3 in figure 5.b), while the kinetic energy is the dominant variable for the cases that manipulate the velocity (case 10 in figure 5.c and case 13 in figure 5.d). The fifth column in figure 6(a) shows that, even in these cases, some improvement can be achieved by including contributions from both the enstrophy and the energy, but that the effect is marginal.

The difference among perturbation methods is best displayed by constructing for each case a conditional ‘template’ for the immediate neighbourhood of the significant cells in the initial unperturbed flow. Figures 7(a,b) include templates for cases 0 and 10, built from the 3×3 -cell neighbourhood of the most significant cell in each experiment. To take into account the reflection and rotational symmetries of the equations of motion, the template is computed by

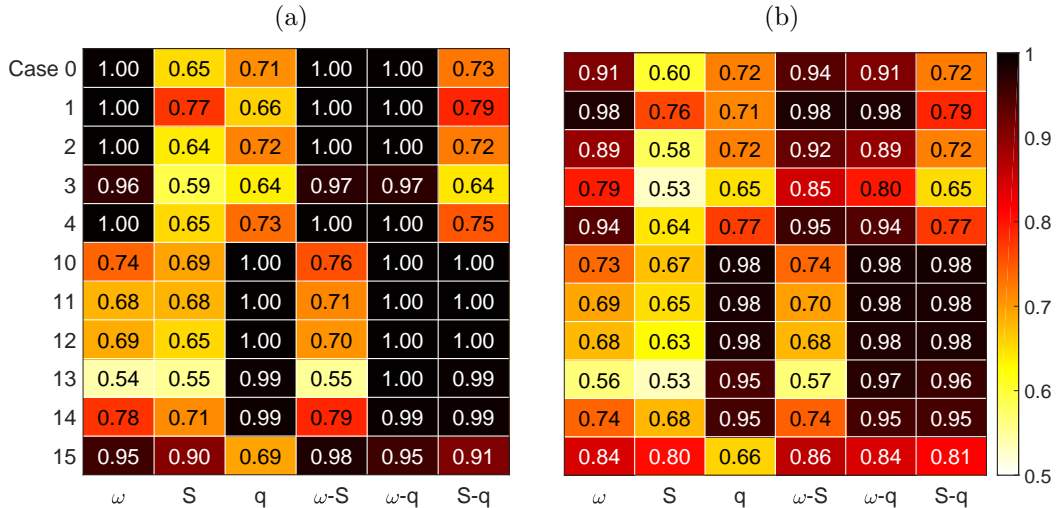


Figure 6: Efficiency of SVM classifiers using different combination of diagnostic variables of the initial cells. Unit efficiency is perfect classification, and 0.5 is random guess. Rows are the cases in table 1, and columns are the different combinations of diagnostic variables. Norm, $\|u\|_2$. (a) $N_c = 10$. (b) $N_c = 6$.

averaging these flow patches after rotating and reflecting them so that they mutually agree as much as possible. To compensate for the effect of the magnitude of the templates, their intensity is scaled to match the global intensity of the flow before comparing them to individual neighbourhoods.

Figure 7(a), which represents the conditional structure in the vicinity of cells that are most sensitive to zeroing their vorticity, is an isolated vortex. This would appear to support the classical view that two-dimensional turbulence is controlled by the interactions among individual vortices [26,27]. But the template in figure 7(b), which corresponds to cells that have been perturbed by zeroing their velocity, and which are thus best diagnosed by the magnitude of their kinetic energy, is a vortex dipole. This is a less expected result, but a reasonable one, because the velocity field of a dipole contains a local jet, and it makes sense that blocking it has a strong effect. In general, the templates for the most significant structures in experiments that manipulate the vorticity, are isolated vortices, while the manipulation of the velocity results in dipoles.

It was mentioned in [11] that case 15 in table 1 is an exception to this rule, because figure 6 shows that, even if this experiment involves manipulating the velocity, its most diagnostic variable is the enstrophy. A little reflection shows the reason. What this experiment does is to substitute the velocity field in the cell by a uniform velocity equal to the average over the original cell. At such, it removes the velocity fluctuations without modifying the mean, and is closer to a vorticity manipulation than to a velocity one. Correspondingly, the conditional template for this case is an isolated vortex.

Figures 7(c,d) show templates conditioned to neighbourhoods of the least significant cells. They are less clear and weaker than the significant ones, and they vary more among different experimental conditions (see §2.1).

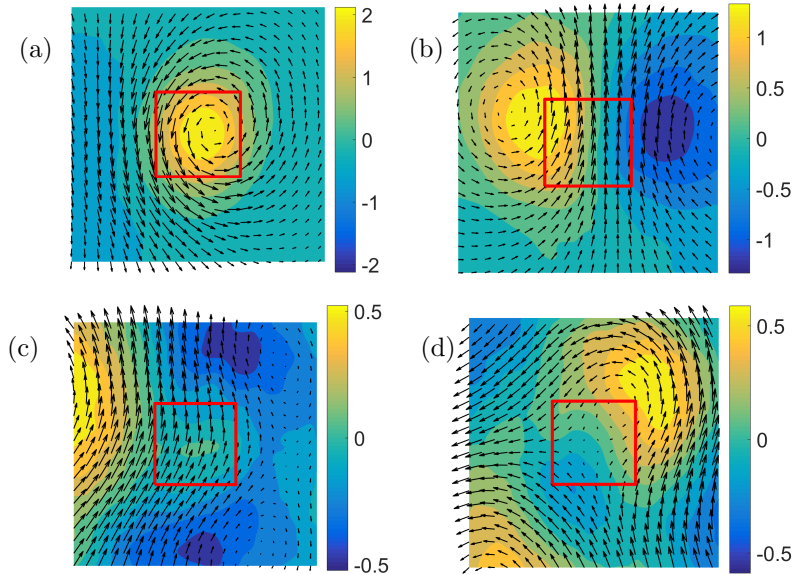


Figure 7: Conditional vorticity and velocity distributions, normalised with their unconditional r.m.s., in the neighbourhood of the most (top row) and least (bottom) significant cells. The test cell is outlined in red and, because of the invariances of the problem, the orientation and the vorticity sign are immaterial. (a,c) Case 0 in table 1. (b,d) Case 10. Compiled from 768 flows, and classified using $\|\mathbf{u}\|_2$.

The classification efficiency and the resulting templates depend on the size of the experimental cells. In general, the efficiency degrades for larger cells, as shown in figure 6 for $N_c = 10$ and $N_c = 6$, and continues to do so for $N_c = 4$ (not shown). In the case of enstrophy, this evolution is consistent with the spectrum in figure 2(b), which shows that the cell size when $N_c = 10$ is of the order of the vortex size, but it is a little surprising that fairly small cells work so well for the kinetic energy, whose spectrum peaks at the scale of the box, suggesting that, at least at this low Reynolds number, the causality of the kinetic energy remains concentrated at the scale of individual vortex pairs (see §3 for a more complete discussion). In fact, the effectiveness of the enstrophy and of the energy behave differently with the cell size. While the mean effectiveness of ω_c^2 as a diagnostic variable in cases 0–4 decays from 0.99 to 0.74 as $N_c = 10 \rightarrow 4$, that of q_c^2 in cases 110–114 only decays from 0.99 to 0.88 in the same range. The templates obtained from coarser experimental grids are similar to those for $N_c = 10$, but become progressively less well defined as N_c decreases.

2.1 Verification

Any result based on the exploitation of large data sets is statistical and, as such, needs to be verified and validated. Verification refers to whether the experimental procedure can be trusted, which mostly has to do with avoiding statistical artefacts. It is discussed in this section. Validation assesses whether the results are relevant to the problem at hand, and is deferred to §2.2.

Template	Template intensity $\ \mathbf{u}_T\ _2/q'_0$	Convergence error (128 – 768)	Approximation error (Flow – Template)
Vortex (case 0)	0.86 – 0.54	0.23 – 0.55	0.71 – 0.98
Dipole (case 10)	0.95 – 0.43	0.21 – 0.42	0.66 – 1.13
Random	0.56	0.37	0.97

Table 2: Measures of approximation error and statistical convergence for the templates in figure 7. The template intensity is $\|\mathbf{u}_T\|_2$, defined over its 3×3 box. The convergence error is defined as the difference between templates computed from 768 and 128 experiments, $\|\mathbf{u}_{T(128)} - \mathbf{u}_{T(768)}\|_2 / \|\mathbf{u}_{T(768)}\|_2$. The approximation error is the difference between the templates and the flow, $\|\mathbf{u} - \mathbf{u}_T\|_2 / \|\mathbf{u}\|_2$. Except for the second column, data are averaged over 768 experiments.

One effect of conditioning can be seen from the difference between the colour bars in figure 7 and those of the full flow in figure 2(a). While the instantaneous vorticity in the latter spans the range $\omega/\omega'_0 \in \pm 3$, the significant templates in figures 7(a,b) only span $\omega/\omega'_0 \in \pm(1-2)$. The r.m.s. intensity, $\|\mathbf{u}_T\|_2/q'_0$, of the different templates is given in the first column of table 2, where the norm is computed over the 3×3 domain of each template in two representative cases (a vortex template in case 0, and a dipole in case 10). The two numbers in each line of this table apply to the templates of the most and least significant cells in each experiment, respectively corresponding to figures 7(a,b) and 7(c,d). Results are essentially the same for other cell modification methods.

The third line in table 2 refers to templates computed from randomly chosen cells, and is similar to the least significant cases in the lines above. It is interesting that the intensities in this line are as high as they are. The naive expectation would be that averaging 768 random cells of individual intensity q' would result in a standard deviation $q'/\sqrt{768} \approx 0.036q'$, but the bottom line of table 2 is ten times higher than this. Clearly, the process of optimally aligning the individual flows while computing the templates creates a template even when there is none. It follows from table 2 that the templates created from the least significant cells are only as good as random, while those for the most significant ones are almost as strong as the unconditional flow.

The second column of table 2 confirms this conclusion. It shows the difference between templates computed from relatively few experiments (128) and those constructed from the full set of experiments (768). For the reasons explained when discussing the template intensity, it is difficult to predict which should be the baseline difference between the results of unrelated experiments, but it is clear from the table that the significant templates – the first of the two numbers in the first two lines – are significantly more converged than the least significant ones, strongly suggesting that the former are physically significant properties, while the latter are not.

The last column in table 2 is the relative approximation error between the flow and the template. As above, the first number in the first two lines is for the most significant templates, and the second one is for the least significant ones. The last line is for random cells, and its approximation error is consistent with the null template that would be obtained from adding independent cells, although we saw above that the random templates are weak, but not null. The approximation errors for the significant cells are lower than random, but still substantial. They show that, although templates are a reasonable approximation to the structure of the flow in the neighbourhood of significant cells, we should not expect to find many ‘pure’ circular

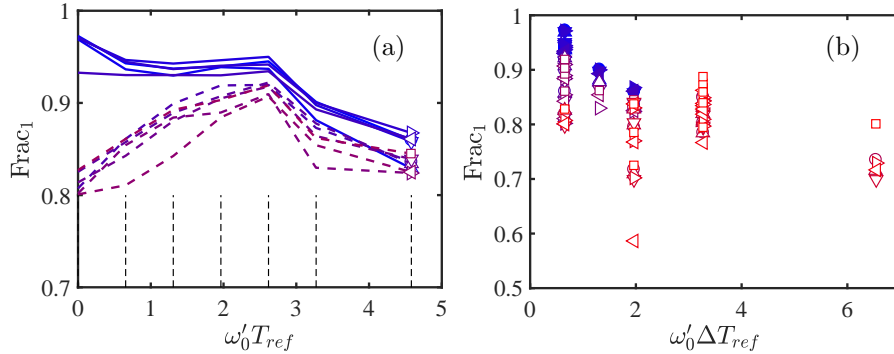


Figure 8: (a) Fraction of cells in the initial flow classified as significant when measured at one test time, and still classified as such at the next test time, as a function of time. Test times are marked by the dashed vertical lines. (b) As in (a), but as a function of the time difference between consecutive test times. Symbols as in table 1, but closed symbols in (b) are vorticity perturbations (cases 0–4) and open symbols are velocity perturbations (cases 10–15). In both figures, the significance norm is $\|\mathbf{u}\|_2$. Lines and symbols as in table 1.

vortices or dipoles in the flow (see figure 2.a).

2.2 Validation

Although it should be clear by now that the templates in figure 7(a,b) contain structural information about the significant flow regions defined above, and that they can be statistically trusted, it remains to be shown that they represent flow properties rather than experimental artefacts. Moreover, although the previous analysis shows that the most significant perturbations are preferentially those which are applied to the neighbourhood of vortices and dipoles, it is unclear whether the converse is also true, and flow regions that can be approximated as vortices and dipoles are preferentially significant.

Consider first the sensitivity of the results to experimental conditions. We have already seen that different experiments produce different templates, but this is not particularly worrisome, and should be considered a desirable property of the Monte-Carlo exploration of possibilities. More disturbing is the dependence on the testing time. The experiments above produce a classification of flow features at time $T = 0$, based on the intensity of their perturbations at a later time, T_{ref} . The choice of T_{ref} is discussed in appendix A, where it is shown that there is a characteristic period, of the order of $\omega'_0 T = 5$, over which causality develops and is preserved. But, even within this constraint, the classification depends on T_{ref} , and it is important to determine whether cells classified as significant for a given T_{ref} remain significant when classified at a different time.

This persistence is checked in figure 8(a), which shows the fraction of cells classified as significant at one of the test times stored by the experiment, which are still classified as such at the next test time. The fraction is high (random sets would only persist 0.25% of the time), and figure 8(b) shows that the decay is mostly a function of the interval among consecutive test times. In agreement with the results in appendix A, figure 8 suggests an effective persistence time of the order of a few turnovers, and indicates that this is the correct time interval over which

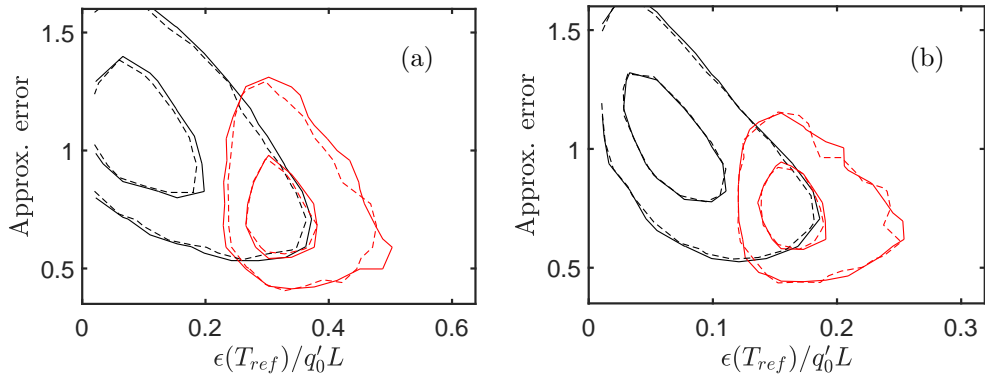


Figure 9: Joint p.d.f. of the relative approximation error, as defined in table 2, versus the experimental divergence at $\omega'_0 T_{ref} = 4.5$. (a) Case 0 in table 1; template is a vortex. (b) Case 10; template is a dipole. Black lines use all the experimental cells. Red lines only use the most significant $n_{keep} = 5$ cells in each experiment. 768 experiments, classified using $\|\mathbf{u}\|_2$. Contours contain 50% and 95% of the probability. —, Tested using the training set; ---, using an independent test set.

to study causality in this flow. The results are approximately independent of the norm used for the classification, although figure 8 shows that vorticity norms are slightly less persistent than velocity ones, and it can be shown that quadratic norms are slightly more persistent than point-wise ones.

The question of whether the relation between templates and significance can be reversed is tested in figure 9, which shows joint p.d.f.s of the approximation error between a template and the flow in the neighbourhood of a cell versus the magnitude of the perturbation resulting from modifying that cell. Contrary to previous figures, the p.d.f.s drawn in black in figure 9 are compiled over all the cells of the original flow, without classification, and it is clear that there is an inverse relation between the two quantities: cells whose flow neighbourhood is better approximated by a significant template are also more causally significant. The p.d.f.s drawn in the figure with red lines only include cells previously classified as most significant. They are the right-most end of the unconditional distributions. The figure displays separately the result of using test data from the set used to train the template, and data from a separate set of experiments, not used in the training. They agree well, decreasing the possibility of template overfitting.

3 Vortices and dipoles

Although a detailed discussion of the dynamics of two-dimensional turbulence is beyond the scope of the present paper, which is mostly concerned with the methodological aspects of how to best collect the information required for scientific discovery, it is still useful to briefly review the physical significance of the collected data.

The most interesting aspect of the above results is the classification of significant structures

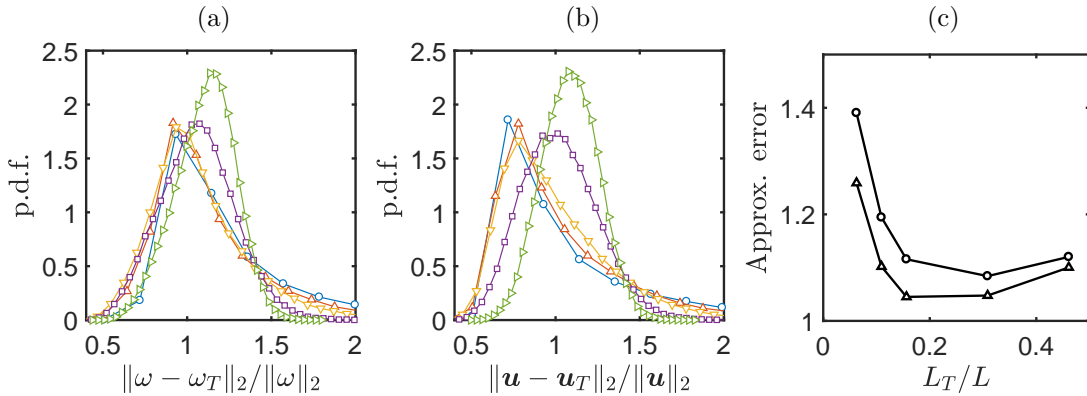


Figure 10: (a,b) P.d.f. of the relative unconditional approximation error between flow and template, as defined in table 2. Templates are scaled to different sizes, L_T , before being fitted to the flow. \circ , $L_T/L = 0.0625$; \triangle , 0.101; ∇ , 0.156; \square , 0.309 (this is the unscaled template from the $N_c = 10$ grid); \triangleright , 0.461. (a) Template is a vortex. (b) Template is a dipole. (c) Average approximation error as a function of L_T . \circ , Vortex template; \triangle , dipole. The template intensity is scaled to match the mean flow intensity.

into vortices and dipoles.

Individual vortices are widely recognised to be the main coherent structures of two-dimensional turbulent flows [26], where they persist because they represent droplets of depleted nonlinearity [34]. But vortex dipoles (‘modons’) have also been investigated as important components of such flows, particularly in geophysics [35,36], where they retain their individuality for long times in the atmosphere and in the ocean. They are also relevant in stratified flows, where they form naturally [16], and in Bose–Einstein condensates [17]. However, although the presence of dipoles in non-rotating two-dimensional turbulence is also well known, they have tended to be considered ‘transient’ structures, whose importance is usually not emphasised [26]. The present results suggest that they deserve a second look. Simulations of a point-vortex gas, which can be viewed as a non-dissipative model for two-dimensional turbulence [28], show that dipoles form spontaneously and suggest that their relevant property in this context is that they carry no net circulation, so that their interaction with the rest of the flow is relatively weak. They are therefore able to move for long distances before being destroyed by collisions with other objects, and they stir the flow in ways similar to neutral particles in a plasma.

It should be clear that, at this stage of the analysis, the templates obtained above should be considered models for flow neighbourhoods, independently of how they were initially obtained, and that we can test how representative of the flow are they without reference to causality tests. This is done in figure 10 for vortices and dipoles. In each case, templates are geometrically scaled to several sizes, since the size at which they optimally fit the flow is a parameter to be determined, rather than assumed. To keep the samples statistically equivalent, each template is fitted to flow neighbourhoods centred at the same $N_c = 10$ test grid, and the resulting p.d.f.s are shown in figures 10(a,b). The mean relative fitting error is given in figure 10(c), and should be compared to those in the third column of table 2, which measures the same quantity between geometrically unscaled templates and cells classified by their significance. Note that the template size, L_T , corresponds in that case to three test cells, so that $L_T/L = 0.309$.

It is interesting that the fitting error in figure 10(c) is lowest at $L_T/L = 0.2$ – 0.4 for both templates, which agrees well with our previous estimates of the size of the structures from the

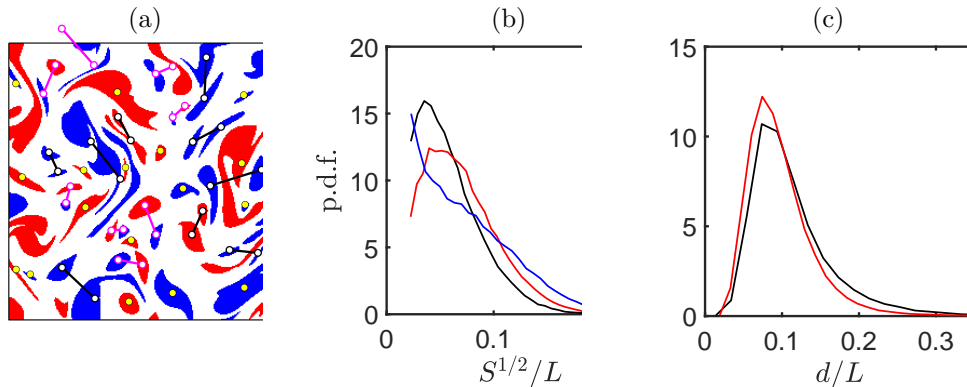


Figure 11: (a) Sample segmented field with pair identification. Blue vortices are counterclockwise, and red ones are clockwise. Black connectors are corrotating pairs, magenta are counterrotating dipoles, and yellow markers are unpaired vortices. Note that, because of their irregular shape, some centres of gravity fall outside their vortex. Vorticity threshold $|\omega| = 0.9\omega'_0$. (b) P.d.f. of the vortex area, S . Black, vortices in corrotating pairs; red, counterrotating dipoles; blue, unpaired vortices. (c) P.d.f. of distance among paired vortices. Symbols as in (b).

significance tests. As explained above, the intensity of the templates has been scaled to match the global intensity of the flow fluctuations, and the message of figure 10(c) is that very small and very large structures of average intensity do not exist. Recall that the cell size was chosen from the flow spectrum, and that it was later confirmed, by testing several test partitions, that the vortex and dipole sizes are comparable to the spectral scale.

To gain a better sense of the prevalence of dipoles in two-dimensional turbulence, figure 11(a) shows a segmentation of a typical flow field into individual positive and negative vortices. Vortices are defined as connected regions in which $|\omega| \geq H\omega'_0$. For very low thresholds, $H \approx 0$, the flow separates into a few large objects that fill the whole box but, as H increases, low-vorticity regions fall below the threshold, and the strong vorticity breaks into more numerous smaller objects. Beyond a certain threshold, the number of vortices decreases again, and eventually vanishes when no vorticity satisfies the thresholding condition. The value $H = 0.9$ in figure 11 is chosen to maximise the number of individual vortices [37]. The vortices in figure 11(a) have been grouped, whenever possible, into co- and counter-rotating pairs. Two vortices are considered a potential pair if their areas differ by less than a factor of m^2 , which is an adjustable parameter. The figure uses $m = 2$, but statistics compiled with $m = 1.5$ and $m = 3$ show no substantial differences. Vortices are paired to the closest unpaired neighbour within their area class, and no vortex can have more than one partner. Some vortices find no suitable partner, and are left unpaired. Statistics compiled over approximately 8500 independent flow fields are given in figures 11(b,c), and show that the vortex area, s , and the distance d between the components of corrotating and counterrotating pairs are very similar. Their averages, $(s^{1/2}/L \approx 0.07)$ and $(d/L \approx 0.1)$, are of the same order as the cell size used in the significance studies. A rough measure of the importance of the pairs is that, out of approximately 5×10^5 vortices, 48% are paired to form dipoles, 24% are in corrotating pairs, and 28% are isolated. Most vortices in the flow are thus in the form of pairs, mostly dipoles. The difference between corrotating and counterrotating pairs is interesting, but it is probably due to the tendency of corrotating pairs to merge into single cores [38], while modons are longer-lasting [35,36].

4 Discussion and conclusions

This paper has explored two related but independent ideas in the context of their use in the process of scientific discovery, with emphasis on turbulence research.

The first idea is the well-known distinction between correlation and causation. We have noted that, because of the difficulty of doing experiments in turbulence (computational or otherwise), research has tended to centre on correlations. The wealth of data generated by direct simulations in the 1990's probably contributed to that trend by creating the illusion that 'we knew everything', and that all questions could be answered.

There are two problems with this illusion. The first one is that, although large data sets contains many answers and, if we believe that turbulence is ergodic, may even contain 'all the answers', the probability of finding them without active researcher participation is vanishingly small. Consider how difficult it would be to study shock waves by tracking the expansion of high-density local condensates in ambient air at equilibrium. Dense-enough condensates are extremely unlikely to form spontaneously, and shocks have to be set up to be studied with any efficiency. The same is true of many intermittent but significant processes in turbulence, especially if we aim at controlling the flow by introducing local out-of-equilibrium perturbations. We noted in the introduction that correlation is the tool of prediction, while causation is the tool of control, and studying control perturbations requires experiments that separate causes from later effects.

The second problem is how to choose which experiments to perform. The classical search for scientific causation is typically hypothesis-driven. The entry point to figure 1 is the second step S2 (i.e., the researcher thinks of a model, and designs experiments to test it). While this 'hypothesis-driven searches' have obvious theoretical appeal, they limit creativity. A model has to be conceived before it can be tested, and paradigm shifts depend on the imagination of the researchers. However, we have noted that faster experimental and computational methods open the possibility of what we have called Monte-Carlo searches (perhaps describable as 'search-driven hypotheses'), in which experiments are performed randomly, and evaluated a posteriori in the hope that some of them may be interesting. This is more expensive than the classical procedure, but may be our best hope of avoiding ingrained prejudice.

We have illustrated these ideas by the application to two-dimensional turbulence in sections §2 and §3, and we can now reflect on how far the hopes expressed above have been realised. The first consideration is cost, which we have already identified as a pacing item for turbulence research. The whole program in this paper took about a month of computer time in a medium-sized department cluster, and was programmed by the author in his spare time over a year. Considerably more time was spent discussing with colleagues what should be done than in actually doing it. Since the effort was conceived as a proof of principle, the problem was purposely chosen small, but more interesting problems are within reach. The basic simulation in §2 runs in about 10 core-seconds, but even a three-dimensional 256^3 simulation of three-dimensional isotropic turbulence can be run in two minutes in a modern GPU. A program to address causality in the three-dimensional turbulence cascade, about which considerably less is known than in two dimensions, can be performed in a modest GPU cluster in a few months [11]. The main roadblock would again be to decide what to do.

The second question is whether something of value has been achieved. As mentioned in the introduction, little was expected from a problem that is usually considered to be essentially

understood. In fact, two previous versions of the present paper [11,31] missed the dipoles completely, and concluded that the experiments confirmed the classical vortex-gas model of two-dimensional turbulence. The dipole template in figure 7(b) was a mildly surprising result of further postprocessing and, if we admit that surprise is one of the defining ingredients of discovery [39], it was a minor discovery, even if we saw in §3 that dipoles were not completely unknown in two-dimensional flows, and that finding them was rather an instance of recalling something that had been forgotten than of discovering something new. This paper is not the place to embark into the development of a dipole model of two-dimensional turbulence, and it should be obvious to anybody familiar with turbulence research that many things need to be done before the paper becomes of independent interest to fluid mechanics. For example, Reynolds number effects have not been considered, and neither has any experiment in actual control. But the fact that something unexpected to the author was found without ‘prompting’ is encouraging for the future of Monte-Carlo methods in problems in which something is genuinely unknown, including applications outside the realm of turbulence.

The third question is what have we learned about the process of data exploitation. It is clear that the scientific method in figure 1 can be seen as an optimisation loop to search for the ‘best’ hypothesis, and it is natural to ask which parts of it can be automated. Our study in sections §2 and §3 was conceived as an experimental test of how far the automation process could be pushed. Several things can be concluded. The first one is that step S1 (observations) can be largely outsourced to the computer, including the reference to ‘asking questions and planning’. The experiments in table 1 were selected (on purpose) with little thought about their significance, although it is difficult to say how much they were influenced by the previous experience of the author. The same can be said about the parts of step S3 that refer to testing predictions against observations. Simulations of two-dimensional turbulence are by now routine, and the classification of the results was outsourced to library programs (figures 5 and 6). An interesting, although not completely unexpected, outcome of the experience has been the importance of verification and validation, as illustrated by the examples in sections §2.1, §2.2 and, up to point, §3. Unexpected problems are probably features of any project involving data analysis, but they are especially dangerous in cases, like the present one, in which the goal is to probe the unknown.

The last point to consider is step S2 in figure 1 (model generation and evaluation), which is the core of the discovery process. Even here, something was automated. The templates in figure 7 are flow models, and were obtained automatically. On the other hand, their interpretation in §3 was entirely manual, and it is difficult to see at the moment how it could be outsourced to a computer. This is not only because of the need for a level of intelligence somewhat above present computer software, but because what are we aiming for is not well defined. If the goal of a scientific project is to find a ‘good’ model, we need to define precisely what we consider a ‘good’ hypothesis. This naturally leads to the influence of the target audience on the definition of the research goal [40]. For a fluid mechanician, the ultimate model of two-dimensional turbulence are the Navier–Stokes equations, and the ultimate cause of any observation are its initial conditions, presumably traceable to the Big Bang. But we mentioned in the introduction that we restrict ourselves here to a shorter time horizon because of some generalised interest in flow control and, while ultimate causality probably remains a meaningless concept [13], causality over a given time interval is well defined. To paraphrase a well-known conundrum, the cause of a chicken over 20 days is an egg, but the cause over 40 days is another chicken. The choice of a temporal interval influences the results and makes them less general, but it makes causality questions and their answers well posed.

The overall conclusion is that human supervision will probably still be required for hypothesis refinement for some time, but that Monte Carlo can contribute something even today. Consider again the interpretation of the scientific method as an optimisation loop to maximise ‘understanding’. As such, if the goal and parameters are well-defined, they could conceivably be incorporated into an automatic optimisation procedure (e.g. a neural network). However, most classical optimisers, including humans, assume local convexity of the cost function, which is at the root of our misgivings about researcher originality and prejudice. Monte Carlo is a different way of looking for a maximum, which, in principle, bypasses the convexity constraint and escapes local maxima by injecting noise in the process [41]. The best use of Monte Carlo science is probably a partially randomised search and classification step, followed by repeated human fine tuning. The hopeful news in fluid mechanics is that doing this is now becoming possible.

Acknowledgement(s)

This work was supported by the European Research Council under the Coturb grant ERC-2014.AdG-669505.

References

- [1] Poincaré H. Science et méthode. Flammarion, Paris; 1920. English translation in Dover books, 1952.
- [2] Kuhn TS. The structure of scientific revolutions. 2nd ed. Chicago U. Press; 1970.
- [3] Nilsson N. Artificial intelligence: a new synthesis. Morgan Kaufmann, San Francisco; 1998.
- [4] Newell A, Simon HA. Computer science as empirical inquiry: Symbols and search. Commun ACM. 1976;19(3):113–126.
- [5] Brooks R. Elephants don’t play chess. Robot Auton Syst. 1990;6:3–15.
- [6] Coveney PV, Dougherty ER, Highfield RR. Big data need big theory too. Phil Trans R Soc A. 2016;374:20160153.
- [7] Succi S, Coveney PV. Big data: the end of the scientific method? Phil Trans R Soc A. 2018;377:20180145.
- [8] Voit EO. Perspective: dimensions of the scientific method. PLoS: Comput Biol. 2019; 15(9):e1007279.
- [9] King P, Rowland J, Aubrey W, et al. The robot scientist Adam. Computer. 2009;42(7):46–54.
- [10] Brenner MP, Eldredge JD, Freund JB. Perspective on machine learning for advancing fluid mechanics. Phys Rev Fluids. 2019;4:100501.
- [11] Jiménez J. Computers and turbulence. Europ J Mech B: Fluids. 2020;79:1–11.
- [12] Mackie J. The cement of the Universe: A study of causation. Oxford U. Press; 1974.

- [13] Russell B. On the notion of cause. *Proc Aristotelian Soc.* 1912;13:1–26.
- [14] Popper KR. Science as falsification. In: *Conjectures and refutations*. Routledge, London; 1963. p. 33–39.
- [15] Maltrud ME, Vallis GK. Energy spectra and coherent structures in forced two-dimensional and beta-plane turbulence. *J Fluid Mech.* 1991;228:321–342.
- [16] Voropayev SI, Afanasyev YD, Filippov IA. Horizontal jets and vortex dipoles in a stratified fluid. *J Fluid Mech.* 1991;227:543–566.
- [17] Neely TW, Samson EC, Bradley AS, et al. Observation of vortex dipoles in an oblate Bose–Einstein condensate. *Phys Rev Lett.* 2010;104:160401.
- [18] Betchov R. An inequality concerning the production of vorticity in isotropic turbulence. *J Fluid Mech.* 1956;1:497–504.
- [19] Kraichnan RH. Inertial ranges in two-dimensional turbulence. *Phys Fluids.* 1967;10:1417–1423.
- [20] Batchelor GK. Computation of the energy spectrum in homogeneous two dimensional turbulence. *Phys Fluids Suppl.* 1969;II, 12:233–239.
- [21] Kraichnan RH. Inertial range transfer in two- and three-dimensional turbulence. *J Fluid Mech.* 1971;47:525–535.
- [22] Onsager L. Statistical hydrodynamics. *Nuovo Cimento Suppl.* 1949;6:279–286.
- [23] Fornberg B. A numerical study of 2-d turbulence. *J Computat Phys.* 1977;25:1–31.
- [24] McWilliams JC. The emergence of isolated coherent vortices in turbulent flow. *J Fluid Mech.* 1984;146:21–43.
- [25] McWilliams JC. A demonstration of the suppression of turbulent cascades by coherent vortices in two-dimensional turbulence. *Phys Fluids A.* 1990;2:547–552.
- [26] McWilliams JC. The vortices of two-dimensional turbulence. *J Fluid Mech.* 1990;219:361–385.
- [27] Carnevale GF, McWilliams JC, Pomeau Y, et al. Evolution of vortex statistics in two-dimensional turbulence. *Phys Rev Lett.* 1991;66:2735–2737.
- [28] Benzi R, Colella M, Briscolini M, et al. A simple point vortex model for twodimensional decaying turbulence. *Phys Fluids A.* 1992;4:1036–1039.
- [29] Kraichnan RH, Montgomery D. Two-dimensional turbulence. *Rep Prog Phys.* 1980;43:547–619.
- [30] Boffetta G, Ecke RE. Two-dimensional turbulence. *Ann Rev Fluid Mech.* 2012;44:427–451.
- [31] Jiménez J. Machine-aided turbulence theory. *J Fluid Mech.* 2018;854:R1.
- [32] LeCun Y, Bengio Y, Hinton G. Deep learning. *Nature.* 2015;521:436–444.
- [33] Cristianini N, Shawe–Taylor J. An introduction to support vector machines and other kernel-based learning methods. Cambridge U. Press; 2000.

- [34] Pushkarev AV, Bos WJT. Depletion of nonlinearity in two-dimensional turbulence. *Phys Fluids*. 2014;26:115102.
- [35] Flierl GR, Larichev VD, McWilliams JC, et al. The dynamics of baroclinic and barotropic solitary eddies. *Dyn Atmos Oceans*. 1980;5:1–41.
- [36] McWilliams JC. An application of equivalent modons to atmospheric blocking. *Dyn Atmos Oceans*. 1980;5:43 – 66.
- [37] Moisy F, Jiménez J. Geometry and clustering of intense structures in isotropic turbulence. *J Fluid Mech*. 2004;513:111–133.
- [38] Meunier P, Le Dizès S, Leweke T. Physics of vortex merging. *C R Physique*. 2005;6:431–450.
- [39] Schaffer S. Making up discovery. In: Boden MA, editor. *Dimensions of creativity*. MIT Press; 1994. p. 13–51.
- [40] Arrieta AB, Díaz-Rodríguez N, Del Ser J, et al. Explainable Artificial Intelligence (XAI): Concepts, taxonomies, opportunities and challenges toward responsible AI. *Inform Fusion*. 2020;58:82–115.
- [41] Deb K, Gupta H. Introducing robustness in multi-objective optimization. *Evol Comput*. 2006;14:463–494.

A Temporal evolution of the perturbation norm

An important parameter of the experiments is the time T_{ref} at which the significance classification is performed, and an estimate of an optimum value can be obtained by checking the evolution of the classification efficiency. A measure of the variability of the effect of perturbing individual cells is given by the ratio between the largest and smallest deviations at T_{ref} , ϵ_M and ϵ_m , expressed as a relative ‘efficiency’

$$\sigma = \frac{\epsilon_M - \epsilon_m}{\epsilon_M + \epsilon_m}, \quad (1)$$

which varies between $\sigma = 0$ for the case in which all perturbations have the same magnitude, to $\sigma = 1$ when the weakest one has zero amplitude. The evolution of this classification efficiency depends on T_{ref} . If the separation into significance classes is done at a given time, and the classification into significance classes is kept constant thereafter, the efficiency typically peaks at T_{ref} , and decreases before and after (see figure 12). It is to be expected that, when σ is measured in this way, it decays to zero at very long times, because the flow fields lose the memory of whether their initial perturbations were more or less influential, and all the experiments tend to identically distributed random decaying flows ($\epsilon_m = \epsilon_M$).

A better indication of the perturbation evolution is obtained if cells are reclassified at each moment, as in figure 13, or as in the evolvent in figure 12. Figure 13 shows that the evolution of σ depends on the perturbation method chosen, but typically peaks at about $\omega'_0 T \approx 5 - 10$, which probably represents the longest time for which the flow retains the memory of the initial conditions. The long-time limit is not $\sigma = 0$ in this case, but a measure of the variability among unrelated turbulent flow fields of similar energy, because the distinction between ϵ_m and

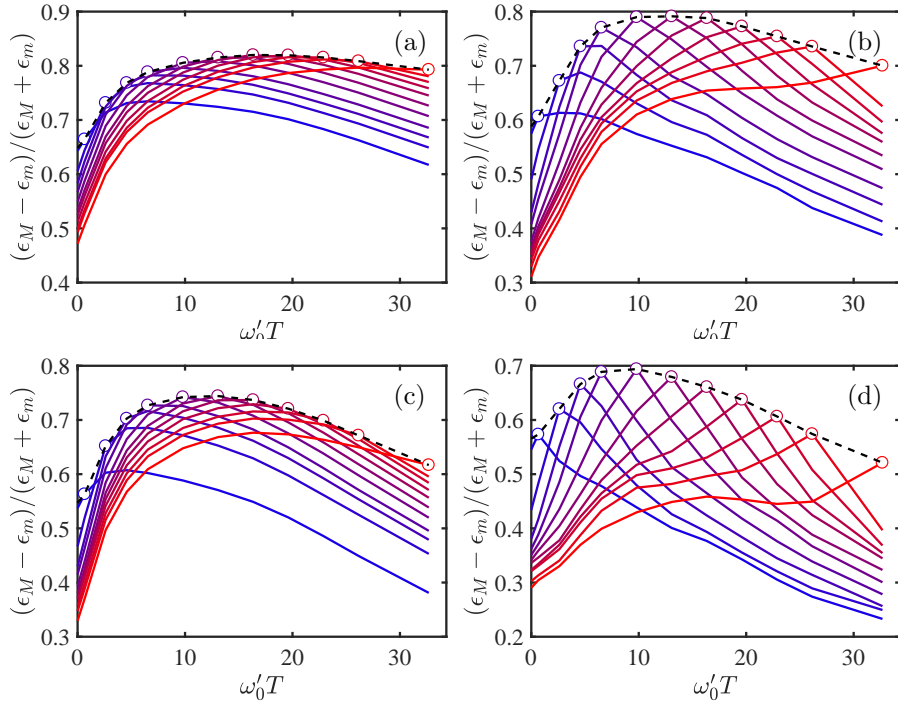


Figure 12: Perturbation significance ratio, as a function of time. All panels reflect case 10 in table 1. The circles mark the time at which the classification of disturbances is made for each curve. The dashed line is the evolut, and correspond to locally classified perturbations, as in figure 13. (a) The norm of the perturbations is $\|\mathbf{u}\|_2$. (b) $\|\mathbf{u}\|_\infty$ (c) $\|\omega\|_2$. (d) $\|\omega\|_\infty$.

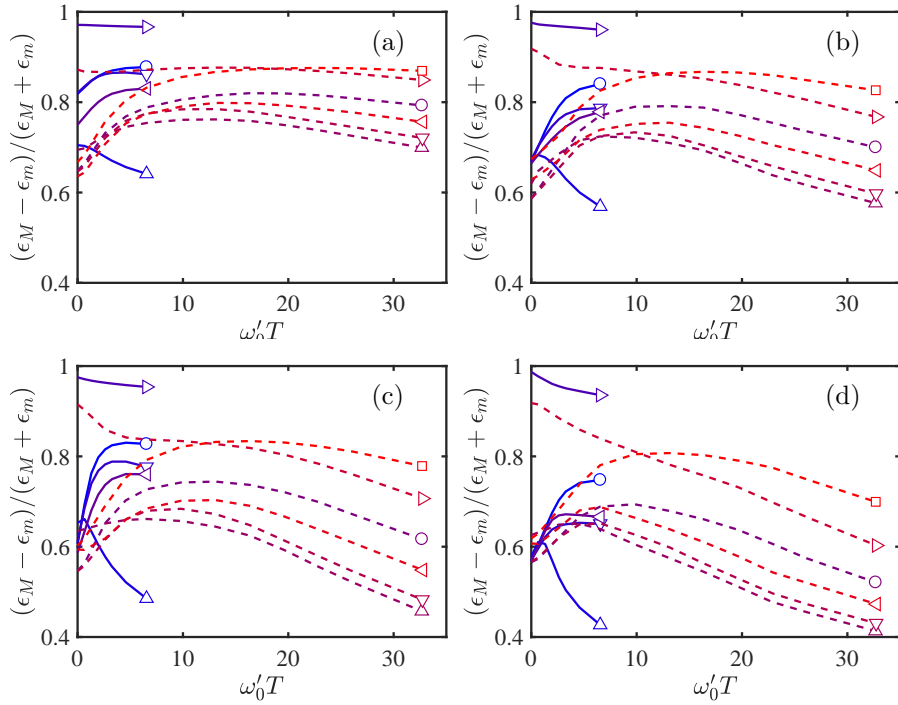


Figure 13: Significance ratio, as a function of time, when the significance classes are redefined at each test time. Symbols as in table 1. (a) Norm of perturbations is $\|\mathbf{u}\|_2$. (b) $\|\mathbf{u}\|_\infty$ (c) $\|\omega\|_2$. (d) $\|\omega\|_\infty$.

ϵ_M is constantly maintained by the classifier. As such, it should presumably be some uniform value, and the slow decay in figure 13 represents the evolution of the Reynolds number in these decaying flows. More interesting is the fast rise, in most experiments, over the initial $\omega'_0 T \approx 5$, which suggests that the initial perturbations need some time to become organised enough to have an effect on the overall norm. It is interesting that some perturbations (cases 1, 4 and 14 in table 1) are created ‘fully formed’, and that their significance decays from the beginning.

Figures 12 and 13 include results with the four norms used in this work. There are substantial differences. As could be expected, $\|\cdot\|_\infty$, which is a local norm, tends to vary more than the integral $\|\cdot\|_2$, but there are also differences between the norms based on the velocity and those based on the vorticity. Independently of the perturbation scheme, the vorticity norms vary more, and their significance ratio grows and decays faster than those of the velocity.

B Vector perturbations

Modifying a vector quantity, such as the velocity, introduces more degrees of freedom than a scalar one, such as the vorticity in two dimensions. In three-dimensional flows, most quantities are vectors, and it is important to reduce the degrees of freedom by estimating which component of the vector would have a greater effect after a given time. Thus, case 10 in table 1 does not consist of zeroing the full velocity vector in the cell, but one of its components, and it is desirable to determine which component to modify for maximum effect.

Assume that we want to modify a column vector property, $\mathbf{u} = \{u_1, u_2\}$, at time $t = 0$ by some amount $\boldsymbol{\delta} = \{\delta_1, \delta_2\}$, and that we would like to choose the direction of $\boldsymbol{\delta}$ so that the effect at time $t = T$ is maximum. We will assume that, although the relation between $\mathbf{u}(0)$ and $\mathbf{u}(T)$ is not linear, the effect of mixing several perturbations can be linearised, so that the perturbation created by $\boldsymbol{\delta}(0) = \alpha_1 \boldsymbol{\delta}^{(1)}(0) + \alpha_2 \boldsymbol{\delta}^{(2)}(0)$ can be approximated as $\boldsymbol{\delta}(T) = \alpha_1 \boldsymbol{\delta}^{(1)}(T) + \alpha_2 \boldsymbol{\delta}^{(2)}(T)$. This is plausible, because $\boldsymbol{\delta}$ is assumed to affect only a small part of the flow. It will be numerically tested below. The goal is to choose the α_j ’s to maximise the quadratic norm $\|\boldsymbol{\delta}(T)\|^2 = (\boldsymbol{\delta}^*(T)|\boldsymbol{\delta}(T))$, where the asterisk denotes Hermitian transpose and $(|)$ is a scalar product. We impose scale by requiring that

$$\|\boldsymbol{\alpha}\|^2 = \alpha_1^2 + \alpha_2^2 = 1. \quad (2)$$

where $\boldsymbol{\alpha} = \{\alpha_1, \alpha_2\}$ is the column vector of coefficients. Assuming linear superposition of the perturbations, it is easy to check that

$$\|\boldsymbol{\delta}(T)\|^2 = \boldsymbol{\alpha}^* \mathbf{A}(T) \boldsymbol{\alpha}, \quad (3)$$

where

$$\mathbf{A} = \begin{pmatrix} (\boldsymbol{\delta}^{(1)*}|\boldsymbol{\delta}^{(1)}) & (\boldsymbol{\delta}^{(1)*}|\boldsymbol{\delta}^{(2)}) \\ (\boldsymbol{\delta}^{(2)*}|\boldsymbol{\delta}^{(1)}) & (\boldsymbol{\delta}^{(2)*}|\boldsymbol{\delta}^{(2)}) \end{pmatrix} \quad (4)$$

is the cross-correlation matrix at time T , and the quantity to be maximised is

$$J(\boldsymbol{\alpha}) = \boldsymbol{\alpha}^* [\mathbf{A}(T) - \lambda \mathbf{I}] \boldsymbol{\alpha}, \quad (5)$$

where \mathbf{I} is the identity matrix, and λ is a Lagrange multiplier to enforce eq:alphanorm. Since \mathbf{A} is Hermitian, all its eigenvalues are real, and the maximum of $\|\boldsymbol{\delta}(T)\|$ is attained by choosing $\boldsymbol{\alpha}$ as the eigenvector of the largest eigenvalue. The procedure can easily be generalised to more dimensions.

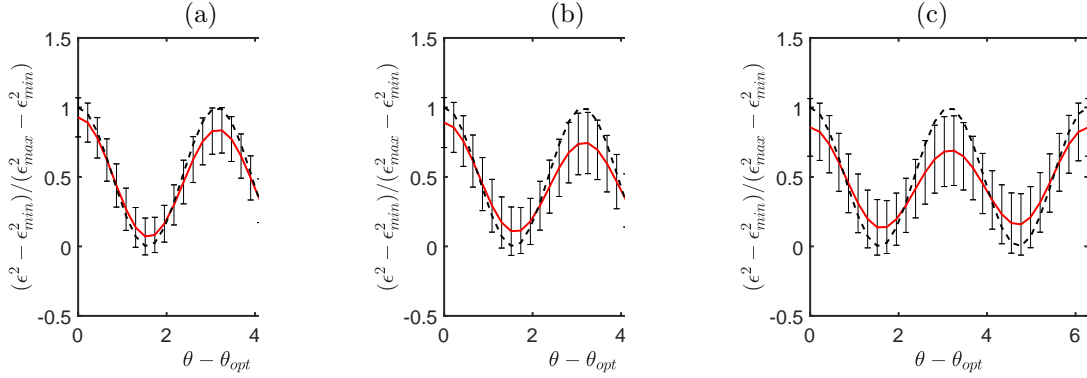


Figure 14: Solid line is the actual $\epsilon = \|u\|_2$ perturbation intensity at time T , as a function of the initial orientation $\theta - \theta_{opt}$ with respect to the linearly determined optimum. Error bars are ± 1 standard deviation. Dashed line is $\hat{\epsilon} = \text{sincos}$. (a) $\omega'_0 T = \omega'_0 T_l = 1.3$. (b) $\omega'_0 T = 2.6$. (c) $\omega'_0 T = 4.5$. Case 10, averaged over 48 different initial fields.

In practice, when manipulating the velocity in the code, the flow is evolved twice for a short time, $\omega'_0 T_l = O(1)$, using each time linearised initial perturbations for one velocity component. For example, if the unperturbed initial condition is $\mathbf{u}_0(0)$, and the initial perturbation resulting from modifying only the u_1 component by some (non-infinitesimal) procedure is \mathbf{b}_1 , the code is first run with the ‘linearisable’ initial condition $\mathbf{u}^{(1)}(0) = \mathbf{u}_0(0) + \eta \mathbf{b}_1$, where, typically, $\eta = 10^{-2}$. The process is repeated with perturbations to the other velocity component. The matrix \mathbf{A} is formed from the observed perturbations $\boldsymbol{\delta}^{(j)}(T_l) = \mathbf{u}^{(j)}(T_l) - \mathbf{u}_0(T_l)$, and the final ‘optimal’ initial condition is chosen to be

$$\mathbf{u}_{opt} = (1 - \alpha_1^{(1)} - \alpha_2^{(1)})\mathbf{u}_0(0) + \alpha_1^{(1)}\mathbf{b}_1(0) + \alpha_2^{(1)}\mathbf{b}_2(0), \quad (6)$$

where $\boldsymbol{\alpha}^{(1)}$ is the eigenvector of the largest eigenvalue, $\lambda^{(1)}$. Note that the linearising factor, η , has been removed from the final perturbation.

In the two-dimensional case, we can express $\boldsymbol{\alpha} = \cos(\theta)\boldsymbol{\alpha}^{(1)} + \sin(\theta)\boldsymbol{\alpha}^{(2)}$. If the initial perturbation is chosen in the direction of a generic $\boldsymbol{\alpha}$, instead of parallel to the linearised optimal eigenvector, the linear prediction is that,

$$\|\boldsymbol{\delta}(T)\|^2 = \cos^2(\theta)\|\boldsymbol{\delta}(T)\|_{max}^2 + \sin^2(\theta)\|\boldsymbol{\delta}(T)\|_{min}^2, \quad (7)$$

where the maximum and minimum are taken over θ . This is tested in figure 14, which shows the degradation of linearity as a function of time. In figure 14(a), which is drawn at the linearisation time T_l , the experimental results follow reasonably closely the theoretical prediction $\hat{\epsilon} = \text{sincos}$, but the agreement gets worse as time progresses. Because of the way the different experiments are normalised in the figure, each of them oscillates between zero and one, but the average does not exactly follow $\hat{\epsilon} = \text{sincos}$ because linear mixing does not exactly hold for nonlinear perturbations, and the optimal orientation does not exactly agree with the linearised prediction. In the limit of zero agreement, the experimental average would tend to a uniform value of 0.5, but it is encouraging that in figure 14(c), which corresponds to the two rightmost flow fields in figure 3 in the text, and which can be considered as fully nonlinear, the maximum averaged perturbation is still at the theoretical linear orientation, and the standard deviation is still moderate.